CARBON letters

Note
Carbon Letters Vol. 18, 84-89 (2016)

High-performance asymmetric supercapacitors based on polyoxometalate-graphene nanohybrids

MinHo Yang[1] and Bong Gill Choi[2,♠]

[1]Department of Nano Bio Research, National NanoFab Center (NNFC), Daejeon 34141, Korea
[2]Department of Chemical Engineering, Kangwon National University, Samcheok 25949, Korea

Key words: polyoxometalate, graphene, ionic liquid, nanohybrid, asymmetric supercapacitor

Article Info

Received 5 January 2016
Accepted 25 February 2016

***Corresponding Author**
E-mail: bgchoi@kangwon.ac.kr
Tel: +82-33-570-6545

Open Access

DOI: http://dx.doi.org/10.5714/CL.2016.18.084

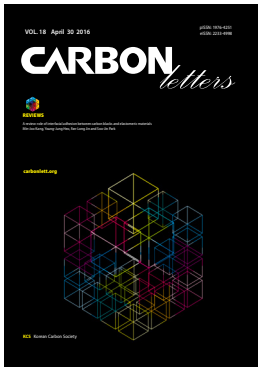

http://carbonlett.org

pISSN: 1976-4251
eISSN: 2233-4998

Supercapacitors (SCs) have attracted much attention as energy storage devices capable of accumulating electricity from renewable sources, as well as deliver high power to smart and portable electronic devices due to their fast dynamic response, high power density, and long cycle-life [1,2]. So far, nanostructured electrodes with pseudocapacitive materials have been widely utilized to enhance the specific capacitance and energy density of supercapcitors [3,4]. However, such materials typically have low electrical conductivity (10^{-5}~10^{-9} S cm^{-1}) [5,6], degrade structurally under rigorous reaction conditions [7], and have a narrow electrochemical window (<1 V) [8,9] which can lead to high internal resistance, large irreversible capacitance loss, and poor rate capability and, consequently, result in supercapacitors with limited power density. A promising strategy to increase power density has been to extend operating cell voltage by taking advantage of an organic electrolyte, or an asymmetric cell configuration [10]. In terms of cost and safety, aqueous asymmetric supercapacitors (ASCs) are a suitable choice for commercial SCs [11]. Aqueous ASCs usually consist of a battery-type Faradic electrode for the energy source and a capacitor-type electrode for the power source, and employ aqueous electrolytes, which can increase cell voltage (up to 2 V) and hence improve both energy and power densities [11,12].

Polyoxometalates (POMs) are attractive Faradic electrode materials because of their remarkable redox activity, structural integrity, and low cost [13-15]. However, POM-based electrodes are electrochemically unstable in aqueous solution due to the dissociation of ionic aggregates [13], which leads to unnecessary loss of specific capacitance. In addition, POM powders have low specific surface areas (<10 m^2 g^{-1}) [16]. Therefore, POMs need to be anchored on an insoluble solid matrix with a high specific surface area to achieve high specific capacitance and stable cycle performance. In this respects, nanocarbons (e.g., carbon nanotubes [17-20] and graphene [21-23]) are good candidates for anchoring POMs. Moreover, their superior electrical conductivity and electrochemical/mechanical stability enable improvement in supercapacitor performance [20,22,23]. However, there has been limited success in utilizing POMs in SCs with satisfactory high specific capacitance and cycle performance, due to limited binding sites and difficulty dispersing the nanocarbons, as well as the weak interaction between POMs and nanocarbons, which still remain a challenge.

Herein, we demonstrate aqueous ASCs based on a POM-graphene nanohybrid with polymeric ionic liquid (POM/PIL/G) as a positive elctrode and activated carbon (AC) as a negative electrode in an aqueous electrolyte of H_2SO_4. The polymeric ionic liquid (PIL) was selected as the surface functionality because of its high binding affinity for the graphene surface, and high ionic conductivity, as well as sufficient binding sites to produce a high density of POMs on the graphene surface. The as-prepared ASC device exhibited high specific capacitance, remarkable rate capability, and excellent cycle stability.

Graphite powder (<20 μm), hydrazine monohydrate, and phosphomolybdic acid hydrate ($H_3PMo_{12}O_{40}{\cdot}xH_2O$) was purchased from Sigma-Aldrich (USA). The ionic liquid, 1-vinyl-3-butylimidazolium bromide ([Vbim][Br]), as a monomer was obtained from C-Tri; azobisisobutyronitrile (AIBN) and chloroform from Junsei (Japan). All chemicals were used as received without further purification.

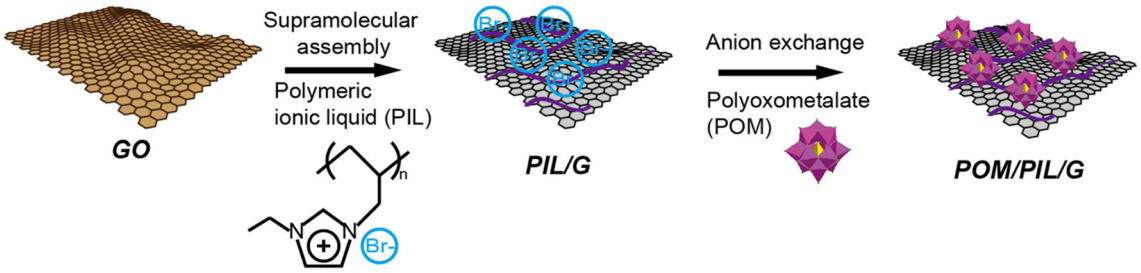

Fig. 1. Schematic illustration of the preparation of the POM/PIL/G nanohybrids.

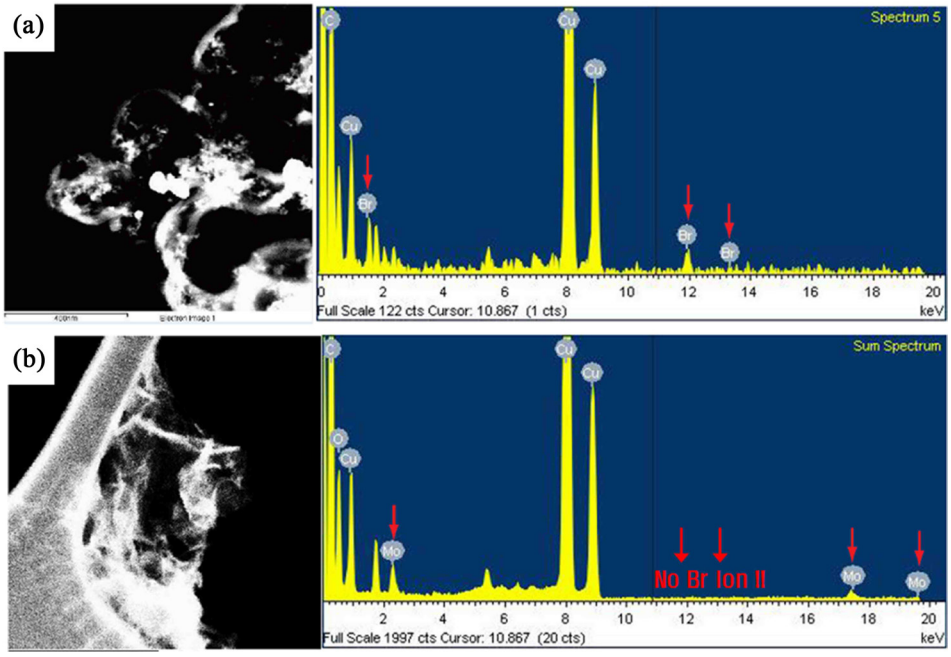

Fig. 2. High-angle annular dark-field scanning transmission electron microscopy (HAADF-STEM) images and energy dispersive X-ray spectroscopy spectra of (a) PIL/G and (b) POM/PIL/G nanohybrids. POM/PIL/G, polyoxometalate-graphene nanohybrid with polymeric ionic liquid.

Prior to preparing the POM/PIL/G, the graphene oxide (GO) and poly(1-vinyl-3-butylimidazolium bromide) were synthesized by a previously reported procedure [24]. To prepare POM/PIL/G, 15 wt% of PIL was completely dissolved in DI water and 20 mg of GO powder added. This mixture was then reduced with hydrazine monohydrate (10 μL) at 90°C for 1 h. After reduction, the dispersion of PIL/G was purified by dialysis to remove unbound PIL, and was collected by filtration. The resulting PIL/G was dispersed in deionize water and mixed with an excess of $H_3PMo_{12}O_{40}{\cdot}xH_2O$ (denoted here POM). The Br^- was substituted with $[PMo_{12}O_{40}]^{3-}$ by anion exchange reaction, resulting in POM/PIL/G nanohybrids.

Transmission electron microscopy (TEM) and high-angle annular dark-field scanning TEM (HAADF-STEM) images and elemental analysis were collected on an E.M. 912 Ω energy-filtering TEM (JEM2100F, JEOL Ltd., Japan) at 200 kV equipped with energy dispersive X-ray spectroscopy (EDS). Cyclic voltammogram was performed with a CHI 760E electrochemical workstation (CH Instruments, USA). The electrochemical impedance spectroscopy measurements were performed over a frequency range from 10^5 to 10^{-2} Hz at sinus amplitude of 10 mV using a VersaSTAT 4 (Princeton Applied Reserch, USA). A cycling stability test was taken by galvanostatic charge/discharge measurements at 50 mV s^{-1} at a scan rate up to 500 cycles. All of the electrochemical measurements were performed in a standard three electrochemical cell with 0.5 M H_2SO_4 aqueous electrolyte at room temperature, and the as-obtained data was within the error range of ±1%. The working electrode was prepared by mixing the active material, acetylene black, and poly(vinylidene difluoride) in a mass ratio of 80:10:10 to form a homogeneous slurry.Then the slurry was coated onto a pretreated stainless steel foil current collector (1 × 1 cm^2) and then dried at 60°C overnight in a vacuum oven. The resulting mass of the coated electrode was ~2 mg. A Pt wire and an Ag/AgCl electrode were used as the counter and reference electrodes, respectively. The AC electrodes were prepared by the same method as the negative electrode describe above. ASCs, AC//POM/PIL/G, were assembled with cellulose film as separator by sandwiching

the AC and POM/PIL/G electrode. The electrolyte was 0.5 M H_2SO_4 aqueous solution.

The preparation of POM/PIL/G as an electrode material for aqueous ASC is illustrated in Fig. 1. First, the PIL was obtained by radical polymerization among vinyl groups of the ionic liquid monomer with the assistance of AIBN. The PIL can be dissolved in water due to the hydrophilicity of the Br^- in the PIL networks, which is responsible for the surface functionalization of the GO sheets in an aqeuous solution. Then, as-prepared GO was modified with the PIL in water and chemically reduced by hydrazine monohydrate. The PIL was attached to the graphene surface by electrostatic and cation-π interactions bewteen the graphene and the imidazolium ring of the PIL [24,25]. Finally, the Br^- anion of the resulting PIL/G was easily replaced by anion exchange reaction to form POM/PIL/G. The anion exchange process between the Br^- and $[PMo_{12}O_{40}]^{3-}$ on the PIL/G surface was confirmed by EDS analysis.

Fig. 2 shows that the Br peaks of PIL/G were completely removed after the ion exchange, and the Mo peaks of POM newly appeared. This result indicates that the POM clusters were successfully immobilized onto the surface of the graphene through electrostatic interaction between the negatively charged POM and positively charged PIL.

Fig. 3 shows the morphology of pristine GO and the POM/PIL/G. As shown in Fig. 3a, the GO exhibits a transparent, layered and wrinkled silk-like structure. After the immobilization of POM on the PIL/G sheet, the graphene surface is decorated with dark spots, indicating the good distribution of the POM clusters (Fig. 3b). From the high magnification TEM image in Fig. 3c, it can be observed that individual POM molecules, with diameters of about 1.5 nm, are separately deposited onto the surface of the PIL/G. Fig 3d shows the coexistence of C and Mo characteristic peaks in POM/PIL/G, which indicates that POM actually exists on the surface.

Cyclic voltammetry (CV) was carried out to evaluate the

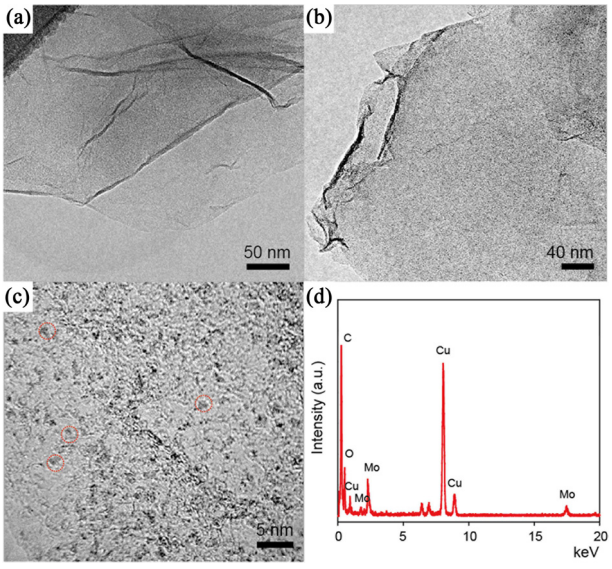

Fig. 3. Transmission electron microscopy images of (a) graphene oxide and (b and c) POM/PIL/G nanohybrids. (d) Energy dispersive X-ray spectroscopy spectrum of POM/PIL/G nanohybrids. The Cu element peak originated from the copper grid. POM/PIL/G, polyoxometalate-graphene nanohybrid with polymeric ionic liquid.

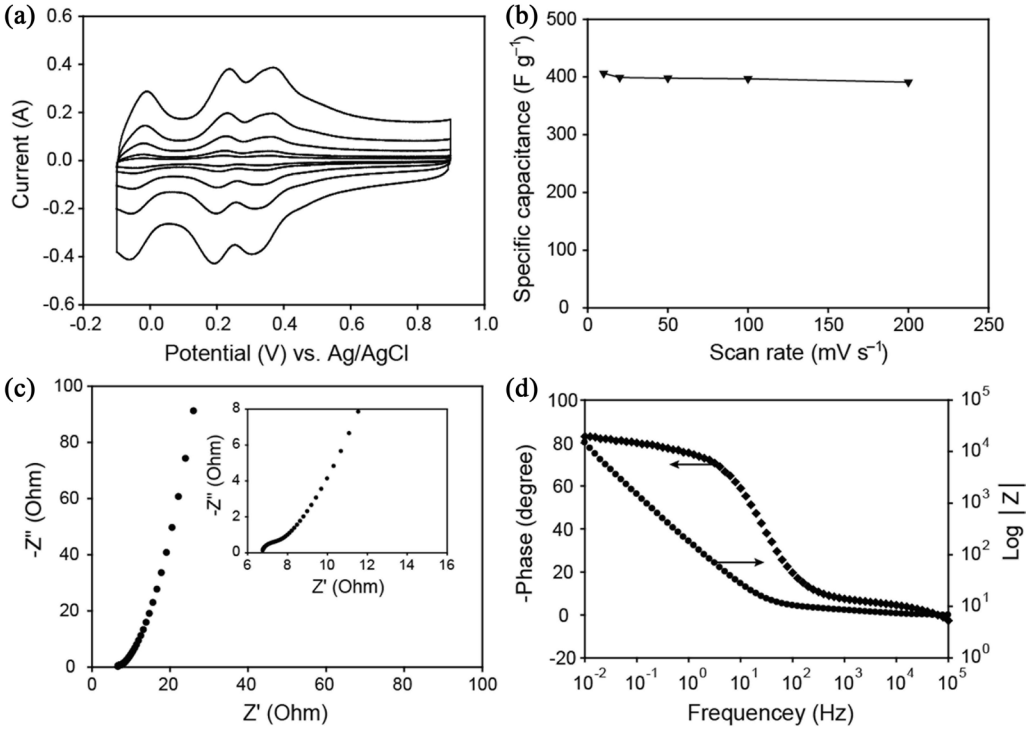

Fig. 4. Electrochemical characterization of POM/PIL/G in 0.5 M H_2SO_4 electrolyte. (a) cyclic voltammetry curves at different scan rates. (b) Plot of specific capacitance versus scan rate. (d) Nyquist plot and (d) Bode plot in the frequency range of 100 kHz to 0.1 Hz. The inset shows the corresponding magnified high frequency region. POM/PIL/G, polyoxometalate-graphene nanohybrid with polymeric ionic liquid.

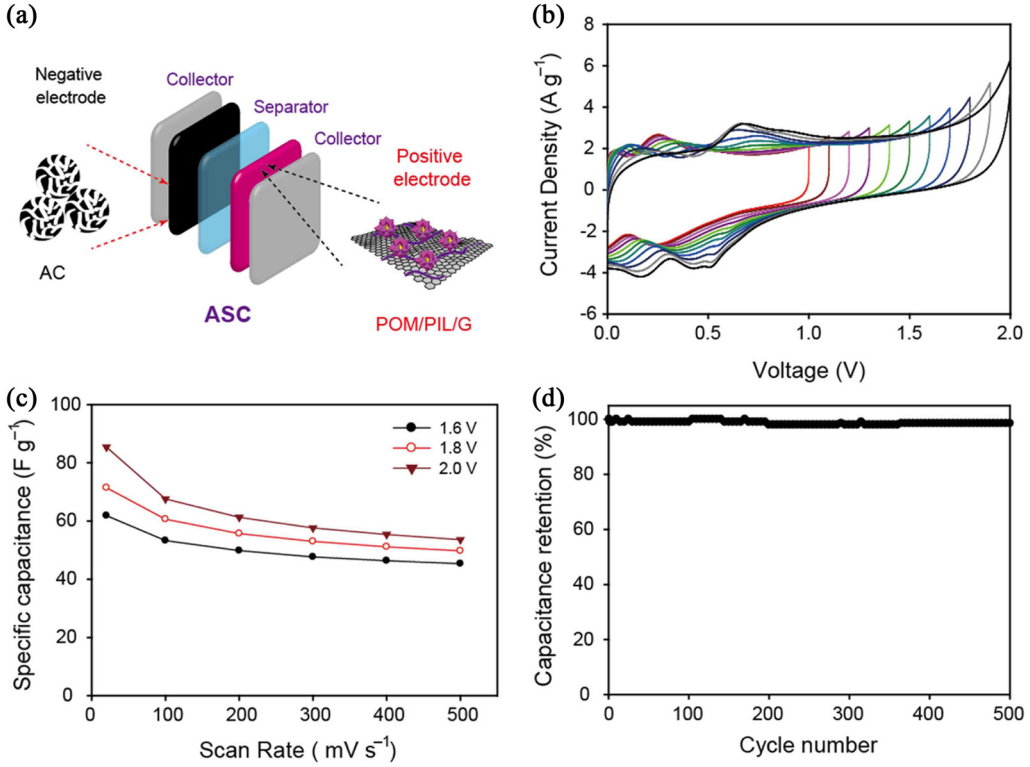

Fig. 5. (a) Schematic illustration of the assembled ASC device, using the POM/PIL/G nanohybrid as the positive electrode and activated carbon as the negative electrode in 0.5 M H_2SO_4 electrolyte. (b) cyclic voltammetry curves measured at different operating cell voltages at a scan rate of 50 mV s^{-1}. (c) Specific capacitance dependence on scan rates at different cell voltages. (d) Cycle stability for the asymmetric supercapacitor devices at a cell voltage of 1.8 V. POM/PIL/G, polyoxometalate-graphene nanohybrid with polymeric ionic liquid.

electrochemical capacitive performance of the as-prepared POM/PIL/G electrode. Fig. 4a displays the CV curves of the POM/PIL/G electrode, measured using three electrode systems in 0.5 M H_2SO_4 electrolyte at different scan rates. Three couples of redox peaks were observed in the CV of the POM/PIL/G, which is indicative of the typical pseudocapacitive behavior of $[PMo_{12}O_{40}]^{3-}$ [13]. The specific capacitance (C_{sp}) was calculated from the voltammetric response based on the following equation [2]: $C_{sp} = \int I(V)dV/(2mv\Delta V)$, where m is the mass of the active electrode material, v is the scan rate, ΔV is the potential window, and $\int I(V)dV$ is the integrated area of the CV curves. From the CV curves of the POM/PIL/G electrode, the specific capacitance was found to be 406 F g^{-1} at 10 mV s^{-1}, and the capacitance was 391 F g^{-1} when the scan rate was increased to 200 mV s^{-1}, retaining 96.3% of its initial value (Fig. 4b).

Electrochemical impedance spectroscopy was further employed to study the electrochemical behavior of the POM/PIL/G electrode. The Nyquist plots for the sample electrodes are presented in Fig. 4c, where the real part (Z′) corresponds to the equivalent of ohmic resistance, and the imaginary part (Z″) reflects the presence of non-resistive elements [26]. The negligible high frequency resistor-capacitor loops or semicircles for electrodes indicate a low faradaic resistance [27]. A short Warburg region, the 45° sloped portion of the Nyquist plot, was observed. These results indicate that the POM/PIL/G electrode has fast electron transport through the conductive graphene sheets, and facile ion diffusion at electrolyte/electrode interface.

Fig. 4d presents a Bode plot of impedance magnitude $|Z|$ and phase over a wide frequency range on a logarithmic scale. It can be observed that the maximum phase angle is about −83°, close to −90° for ideal capacitive behavior [28]. The capacitor response frequency, f_0, at the phase angle of −45° was about 22 Hz and the relaxation time constant τ_0 was calculated to be about 0.05 s by the equation $\tau_0 = 1/f_0$.

Considering the high specific capacitance of the POM/PIL/G, an asymmetric supercapacitor was fabricated using the POM/PIL/G as the positive electrode and the AC as the negative electrode with 0.5 M H_2SO_4 electrolyte (Fig. 5a). In order to obtain maximal cell operating voltage, the loading mass of the positive and negative electrodes was balanced. The loading mass ratio between the positive and negative electrodes was calculated to be 4.64, following equation [2]: $m+/m- = (C- \times \Delta V-)/(C+ \times \Delta V+)$, where m is the mass, C is the specific capacitance and ΔV is the potential windows of the individual positive and negative electrodes.

Fig. 5b shows CV curves at different working voltages for the assembled AC//POM/PIL/G asymmetric supercapacitor. The data proved that the stable electrochemical window can be extended up to 2.0 V. The distorted rectangular CV curves were attributed to the contribution of the pseudocapacitive behavior of the positive electrode.

The specific capacitances for operating voltages of 1.6, 1.8, and 2.0 V at different scan rates calculated from the CV curves are presented in Fig. 5c. The specific capacitance at

20 mV s^{-1} was 61.9, 71.4, and 85.4 F g^{-1} for 1.6, 1.8, and 2.0 V, respectively. In addition, the capacitance values at voltage windows of 1.6, 1.8, and 2.0 V remained 61%, 71%, and 85% of the initial capacitance, respectively.

A cycling test of over 500 cycles for the AC//POM/PIL/G asymmetric supercapacitor was carried out. Fig. 5d shows the specific capacitance retention as a function of cycling numbers, with only 1.5% loss in the specific capacitance after 500 charge-discharge cycles.

We prepared nanohybrids of POM and graphene with PIL through a simple fabrication method in aqueous solution and demonstrated their capacitive behaviors in both symmetric and asymmetric configurations with 0.5 M H_2SO_4 aqeuous electrolyte. The PIL-modified graphene allows the high dispersion of individual POM molecules on the graphene surface through electrostatic interactions, which leads to remarkable charge transfer activity and pseudocapacitive behaviors. After optimization, the ASC device using POM/PIL/G and AC as positive and negative electrodes, respectively, exhibited extended cell voltage up to 2.0 V, specific capacitance of 85.4 F g^{-1} at a cell voltage of 2.0 V, and stable cycling performance with 98.5% capacitance retention after 500 cycles.

Conflict of Interest

No potential conflict of interest relevant to this article was reported.

Acknowledgements

This work was supported by the National Research Foundation of Korea (NRF) Grant funded by the Korean Government (MSIP) (No. 2015R1C1A1A02036556).

References

[1] Armaroli N, Balzani V. Towards electricity-powered world. Energy Environ Sci, **4**, 3193 (2011). http://dx.doi.org/10.1039/c1ee01249e.

[2] Achilleos DS, Hatton TA. Surface design and engineering of hierarchical hybrid nanostructures for asymmetric supercapacitors with improved electrochemical performance. J Colloid Interface Sci, **447**, 282 (2015). http://dx.doi.org/10.1016/j.jcis.2014.12.080.

[3] Simon P, Gogotsi Y. Materials for electrochemical capacitors. Nat Mater, **7**, 845 (2008). http://dx.doi.org/10.1038/nmat2297.

[4] Lu Q, Chen JG, Xiao JQ. Nanostructured electrodes for high-performance pseudocapacitors. Angew Chem Int Ed, **52**, 1882 (2013). http://dx.doi.org/10.1002/anie.201203201.

[5] Motori A, Sandrolini F, Davolio G. Electrical properties of nickel hydroxide for alkaline cell systems. J Power Sources, **48**, 361 (1994). http://dx.doi.org/10.1016/0378-7753(94)80032-4.

[6] Lang XY, Fu HY, Hou C, Han GF, Yang P, Liu YB, Jiang Q. Nanoporous gold supported cobalt oxide microelectrodes as high-performance electrochemical biosensors. Nat Commun, **4**, 2169 (2013). http://dx.doi.org/10.1038/ncomms3169.

[7] Wang G, Liu H, Horvat J, Wang B, Qiao S, Park J, Ahn H. Highly ordered mesoporous cobalt oxide nanostructures: synthesis, characterisation, magnetic properties, and applications for electrochemical energy devices. Chem Eur J, **16**, 11020 (2010). http://dx.doi.org/10.1002/chem.201000562.

[8] Liu J, Jiang J, Cheng C, Li H, Zhang J, Gong H, Fan HJ. Co_3O_4 nanowire@MnO_2 ultrathin nanosheet core/shell arrays: a new class of high-performance pseudocapacitive materials. Adv Mater, **23**, 2076 (2011). http://dx.doi.org/10.1002/adma.201100058.

[9] Xie J, Sun X, Zhang N, Xu K, Zhou M, Xie Y. Layer-by-layer β-$Ni(OH)_2$/graphene nanohybrids for ultraflexible all-solid-state thin-film supercapacitors with high electrochemical performance. Nano Energy, **2**, 65 (2013). http://dx.doi.org/10.1016/j.nanoen.2012.07.016.

[10] Augustyn V, Simon P, Dunn B. Pseudocapacitive oxide materials for high-rate electrochemical energy storage. Energy Environ Sci, **7**, 1597 (2014). http://dx.doi.org/ 10.1039/c3ee44164d.

[11] Wang F, Xiao S, Hou Y, Hu C, Liu L, Wu Y. Electrode materials for aqueous asymmetric supercapacitors. RSC Adv, **3**, 13059 (2013). http://dx.doi.org/10.1039/c3ra23466e.

[12] Khomenko V, Raymundo-Piñero E, Béguin F. Optimisation of an asymmetric manganese oxide/activated carbon capacitor working at 2 V in aqueous medium. J Power Sources, **153**, 183 (2006). http://dx.doi.org/10.1016/j.jpowsour.2005.03.210.

[13] Sadakane M, Steckhan E. Electrochemical properties of polyoxometalates as electrocatalysts. Chem Rev, **98**, 219 (1998). http://dx.doi.org/10.1021/cr960403a.

[14] López X, Carbó JJ, Bo C, Poblet JM. Structure, properties and reactivity of polyoxometalates: a theoretical perspective. Chem Soc Rev, **41**, 7537 (2012). http://dx.doi.org/10.1039/c2cs35168d.

[15] Park S, Lian K, Gogotsi Y. Pseudocapacitive behavior of carbon nanoparticles modified by phosphomolybdic acid. J Electrochem Soc, **156**, A921 (2009). http://dx.doi.org/10.1149/1.3223964.

[16] Kim H, Jung JC, Song IK. Chemical immobilization of heteropolyacid catalyst on inorganic mesoporous material for use as an oxidation catalyst. Catal Surv Asia, **11**, 114 (2007). http://dx.doi.org/10.1007/s10563-007-9025-1.

[17] Ma D, Liang L, Chen W, Liu H, Song YF. Covalently tethered polyoxometalate–pyrene hybrids for noncovalent sidewall functionalization of single-walled carbon nanotubes as high-performance anode material. Adv Funct Mater, **23**, 6100 (2013). http://dx.doi.org/10.1002/adfm.201301624.

[18] Giusti A, Charron G, Mazerat S, Compain JD, Mialane P, Dolbecq A, Rivière E, Wernsdorfer W, Biboum RN, Keita B, Nadjo L, Filoramo A, Bourgoin JP, Mallah T. Magnetic bistability of individual single-molecule magnets grafted on single-wall carbon nanotubes. Angew Chem Int Ed, **48**, 4949 (2009). http://dx.doi.org/10.1002/anie.200901806.

[19] Kawasaki N, Wang H, Nakanishi R, Hamanaka S, Kitaura R, Shinohara H, Yokoyama T, Yoshikawa H, Awaga K. Nanohybridization of polyoxometalate clusters and single-wall carbon nanotubes: applications in molecular cluster batteries. Angew Chem Int Ed, **50**, 3471 (2011). http://dx.doi.org/10.1002/anie.201007264.

[20] Akter T, Hu K, Lian K. Investigations of multilayer polyoxometalates-modified carbon nanotubes for electrochemical capacitors. Electrochim Acta, **56**, 4966 (2011). http://dx.doi.org/10.1016/j.electacta.2011.03.127.

[21] Kume K, Kawasaki N, Wang H, Yamada T, Yoshikawa H, Awaga K. Enhanced capacitor effects in polyoxometalate/graphene nanohybrid materials: a synergetic approach to high performance

energy storage. J Mater Chem A, **2**, 3801 (2014). http://dx.doi.org/10.1039/c3ta14569g.

[22] Kim Y, Shanmugam S. Polyoxometalate−reduced graphene oxide hybrid catalyst: synthesis, structure, and electrochemical properties. ACS Appl Mater Interfaces, **5**, 12197 (2013). http://dx.doi.org/10.1021/am4043245.

[23] Suárez-Guevara J, Ruiz V, Gómez-Romero P. Stable graphene–polyoxometalate nanomaterials for application in hybrid supercapacitors. Phys Chem Chem Phys, **16**, 20411 (2014). http://dx.doi.org/10.1039/c4cp03321c.

[24] Yang M, Choi BG, Jung SC, Han YK, Huh YS, Lee SB. Polyoxometalate-coupled graphene via polymeric ionic liquid linker for supercapacitors. Adv Funct Mater, **24**, 7301 (2014). http://dx.doi.org/10.1002/adfm.201401798.

[25] Zhang Y, Shen Y, Yuan J, Han D, Wang Z, Zhang Q, Niu L. Design and synthesis of multifunctional materials based on an ionic-liquid backbone. Angew Chem Int Ed, **45**, 5867 (2006). http://dx.doi.org/10.1002/anie.200600120.

[26] Rubinson JF, Kayinamura YP. Charge transport in conducting polymers: insights from impedance spectroscopy. Chem Soc Rev, **38**, 3339 (2009). http://dx.doi.org/10.1039/b904083h.

[27] Portet C, Lillo-Ródenas MÁ, Linares-Solano A, Gogotsi, Y. Capacitance of KOH activated carbide-derived carbons. Phys Chem Chem Phys, **11**, 4943 (2009). http://dx.doi.org/10.1039/B816514A.

[28] Sheng K, Sun Y, Li C, Yuan W, Shi G. Ultrahigh-rate supercapacitors based on eletrochemically reduced graphene oxide for ac line-filtering. Sci Rep, **2**, 247 (2012). http://dx.doi.org/10.1038/srep00247.